Please cite this article in press as: Montel et al., A Multiparametric and High-Throughput Assay to Quantify the Influence of Target Size on Phagocytosis, Biophysical Journal (2019), https://doi.org/10.1016/j.bpj.2019.06.021

Biophysical *Journal*
Article

Biophysical Society

A Multiparametric and High-Throughput Assay to Quantify the Influence of Target Size on Phagocytosis

Lorraine Montel,[1,3] Léa Pinon,[1,2,3] and Jacques Fattaccioli[1,3,*]
[1]PASTEUR, Département de Chimie, École Normale Supérieure, PSL University, Sorbonne Université, CNRS, Paris, France; [2]Institut Curie, PSL University, INSERM U932, Paris, France; and [3]Institut Pierre-Gilles de Gennes pour la Microfluidique, Paris, France

ABSTRACT Phagocytosis by macrophages represents a fundamental process essential for both immunity and tissue homeostasis. It consists in the uptake of pathogenic or cellular targets larger than 0.5 μm. For the biggest particles, the phagocytic process involves a massive reorganization of membrane and actin cytoskeleton as well as an important intracellular deformation all in a matter of minutes. The study of the role of the size of objects in their phagocytosis has led to contradictory results in the last decades. We designed a method using confocal microscopy, automated image analysis, and databases for fast quantitative analysis of phagocytosis assays. It yields comprehensive data on the cells and targets geometric and fluorescence intensity parameters, automatically discriminates internalized from external targets, and stores the relationship between a cell and the targets it has engulfed. We used two types of targets (solid polystyrene beads and liquid lipid droplets) to investigate the influence of size on the phagocytic uptake of macrophages. The method made it possible not only to perform phagocytic assays with functionalized droplets and beads of different sizes but to use polydisperse particles to further our understanding of the role of size in phagocytosis. The use of monodisperse and polydisperse objects shows that whereas smaller monodisperse objects are internalized in greater numbers, objects of different sizes presented simultaneously are internalized without preferred size. The total surface engulfed by the cell is thus the main factor limiting the uptake of particles, regardless of their nature or size. A meta-analysis of the literature reveals that this dependence in surface is consistently conserved throughout cell types, targets' nature, or activated receptors.

SIGNIFICANCE Phagocytosis by macrophages represents a fundamental process that consists in the uptake of pathogenic or cellular targets. The study of the role of the size of objects in their phagocytosis has led to contradictory results in the last decades. To address this question, we designed a comprehensive, semiautomated, and quantitative phagocytic assay in conjunction with two types of microparticles showing monodisperse or polydisperse size distribution. We show that size is not a limiting factor of phagocytosis but that phagocytosis depends on the total amount of surface area a cell is able to produce.

INTRODUCTION

Phagocytosis by macrophages represents a fundamental process essential for both immunity and tissue homeostasis. It consists in the uptake of pathogenic or cellular targets larger than 0.5 μm. For the biggest particles, the phagocytic process involves a massive reorganization of membrane and actin cytoskeleton as well as an important intracellular deformation all in a matter of minutes (1). The influence of biological (2–6), chemical (7–9), and physical (10–13) parameters of the targets on their phagocytosis has been evaluated and compared to unravel the mechanisms of internalization. The main parameter used to assess the efficiency of phagocytosis is the phagocytic index, a tool created by Leishman (14), that quantifies the phagocytic process by measuring the average number of internalized objects per phagocyte. Initially, the measurements were performed by counting both cells and targets under a microscope. Since then, methods were devised to obtain the phagocytic index directly from a population of phagocytes, such as spectrophotometry (15–17) or cytometry (18,19), and more recently, the counting of cells and targets on microscopy

Submitted January 11, 2019, and accepted for publication June 17, 2019.
*Correspondence: jacques.fattaccioli@ens.fr
Editor: Ana-Suncana Smith.
https://doi.org/10.1016/j.bpj.2019.06.021

Please cite this article in press as: Montel et al., A Multiparametric and High-Throughput Assay to Quantify the Influence of Target Size on Phagocytosis, Biophysical Journal (2019), https://doi.org/10.1016/j.bpj.2019.06.021

images began to be automatized (20–25). All of them rely on a fluorescent staining of cells and targets to count the number of internal targets and cells and compute the phagocytic index. In addition, the most recent (24,25) provides morphologic measurements on the cells that can then be correlated to the individual number of particles internalized. Phagocytic index, despite its simplicity, is a quantitation averaged over a whole cell population. It is hence not able to capture the full details of the process at the individual level of the cells. The phagocytic index relies on the assumption that all the particles are identical and is thus inadequate to analyze the phagocytosis of diverse targets in a competitive context.

The influence of the size of the targets on the phagocytic efficiency has been studied for more than 50 years (15–19,26–29) for diameters ranging from 100 nm to tens of micrometers. However, experimental results performed with monodisperse particles and published in the literature are contradictory. In some cases, an optimal size for particle uptake seems to emerge (18,27), whereas in others (15,19,28), the number of internalized particles is higher for smaller targets as compared to larger ones in a totally monotonous manner. In some cases, the phagocytic index varies by one order of magnitude for apparently similar experimental conditions reported in two different articles from the literature (16,18,19,27). Using polydisperse targets could provide new insights about the question of size. However, the phagocytic index, as an averaged quantitation, is inadequate for assessing the phagocytosis of polydisperse droplets. An algorithm that registers the relationships between the targets and their size and the cells that have internalized them is required to evaluate the role of size in the competitive phagocytosis of polydisperse targets.

Herein, we have designed a semiautomatic quantitation procedure for image analysis based on confocal microscopy pictures, yielding comprehensive results on the shape, size, and fluorescence intensity for both cells and targets (Fig. 1). Because fluorescent immunoglobulins G (IgGs) on the liquid interface of droplets form clusters and are extracted after internalization, the detection strategy of targets had to be performed on bright-field images, unlike most previous methods from the literature. And because our aim is to relate each cell with the targets within, the cells needed to be segmented from a nuclear and cytoplasmic stain. With the aim to answer complex biological questions, results are stored in a relational database that keeps track of all the relationships between cells and targets and records morphological or biochemical features for each object of the experiment. The method allows relating each cell with its internalized targets in a bidirectional way, hence recording all the available information of a particular experimental condition, where previous methods could only provide morphological measurements on the cells. Because the segmentation of particles does not require staining, the assessment of the phagocytosis of unaltered particles is possible. A schematic view of the process is schematized in Fig. 1.

We performed experiments with both monodisperse and polydisperse targets, with and without opsonization, and confronted them with results from the literature about the role of size in phagocytosis. Using the insight provided by the behavior of macrophages toward polydisperse targets, we conclude that the availability of cell membrane surface is the limiting parameter governing phagocytic uptake, regardless of target size. Cells internalize targets indiscriminately until they reach a total internalized surface that differs between nonspecific and FcγR-mediated phagocytosis.

MATERIALS AND METHODS

Materials

Soybean oil (Chemical Abstracts Service (CAS) no. 8001-22-7), Pluronic F-68 (CAS no. 9003-11-6), Tween 20 (CAS no. 9005-64-5), sodium

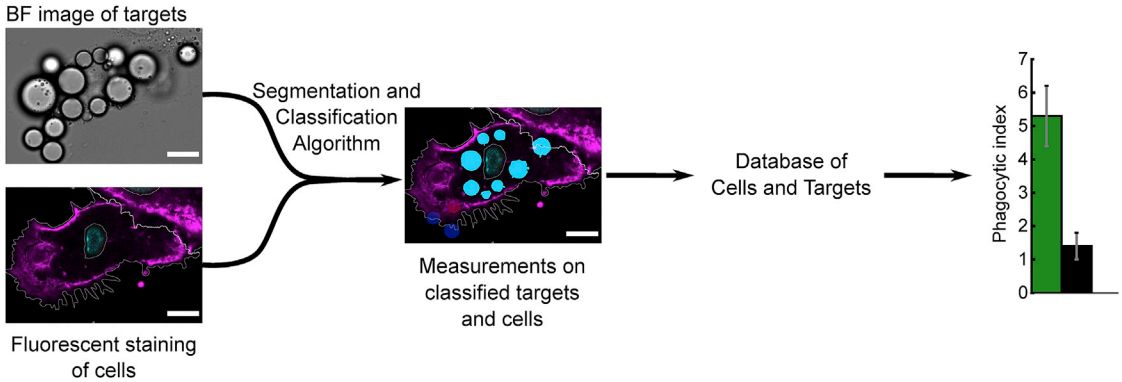

FIGURE 1 Schematic representation of the data obtained by the automatic detection of phagocytosis. The targets and the cells are detected on the images (classified and measured). The results of the measurements and classification are stored into a relational database in which the measurement of the cells, measurement of the targets, and the relationship between the targets and the cell are stored. Complex data can be extracted and plotted from this database. To see this figure in color, go online.

Please cite this article in press as: Montel et al., A Multiparametric and High-Throughput Assay to Quantify the Influence of Target Size on Phagocytosis, Biophysical Journal (2019), https://doi.org/10.1016/j.bpj.2019.06.021

alginate (CAS no. 9005-38-3), and dimethyl sulfoxide (DMSO) were purchased from Sigma-Aldrich (Saint-Quentin-Fallavier, France). Lipiodol (CAS no. 8002-46-8) was a kind gift of the company Guerbet (Villepinte, France). DSPE-PEG2000-biotin (1,2-distearoyl-sn-glycero-3-phospho ethanolamine-N-[biotinyl(polyethylene glycol)-2000]) were purchased from Avanti Polar Lipids (Alabaster, AL). Alexa-Fluor-488-conjugated mouse antibiotin IgGs (reference (ref) 200-542-211) were purchased from Jackson ImmunoResearch Laboratories (West Grove, PA). Polybead microspheres (ref 17134-15, 07312-5, and 17136-5) were purchased from PolySciences (Hirschberg, Germany).

Emulsion fabrication

We first disperse by manually stirring 15 g of soybean oil in an aqueous phase containing 2.5 g of a surfactant (poloxamer F-68, initial proportion of 30% w/w) and 2.5 g of a thickening agent (sodium alginate, initial proportion of 4% w/w). This crude, polydisperse emulsion is further sheared and rendered quasimonodisperse in a Couette cell apparatus under a controlled shear rate, following the method developed by Mason and Bibette (30). The value of the shear rate determines the size distribution of droplets. Before decantation, the emulsion is diluted to have a proportion of 1% w/w of poloxamer F-68 and 5% w/w of oil. After one night of decantation, the dispersed phase is diluted with a solution of poloxamer F-68 with an initial proportion of 1% w/w. After several decantation steps to remove very small droplets, the emulsion (final proportion of 50% w/w of oil) is stored at 12°C in a Peltier cooled cabinet. Size distributions of the emulsion samples are reported in Fig. S1.

Emulsion functionalization

The extended version of the functionalization method has already been published (31) and is summarized shortly hereafter. The desired quantity of droplets is washed three times with a solution of Tween 20 at critical micelle concentration (CMC) (0.06 g/L) in phosphate buffer saline (PBS). The quantity of DSPE-PEG2000-biotin required is calculated to be 100 times the number of molecules necessary to saturate the total surface of droplets based on a minimal occupied area of 12.6 nm^2 per phospholipid (32). That amount of DSPE-PEG2000-biotin saturates the surface of droplets as to prevent the formation of clusters at the surface when the droplets touch a cell. DSPE-PEG2000-biotin is diluted in DMSO to a total volume of 20 μL and mixed with Tween 20 at CMC in PBS and washed droplets for a total volume of 200 μL. The suspension is incubated for 90 min in agitation at room temperature. Afterward, the remaining phospholipids and DMSO are diluted at least 10,000 times through 4 washing steps with Tween 20 at CMC in PBS. Droplets are then resuspended with antibiotin Alexa 488 antibodies (ref 200-542-211; Jackson ImmunoResearch Laboratories) in PBS/Tween20 CMC solution, with antibodies in a 1:1 ratio compared to the DSPE-PEG2000-biotin available on the total surface of the droplets and incubated for 45 min at room temperature. Remaining antibodies are diluted at least 2000 times through 3 washing steps with PB/Tween 20 0.007% w/w. PB/Tween 20 is then removed by a final centrifugation step and droplets are resuspended in 40 μL/coverslip DMEM 4.5 g/L L-glucose without phenol red at 37°C.

Polystyrene beads functionalization

The desired quantity of beads (2 million per coverslip) is washed three times with PBS (ref 14190250; Life Technologies, Carlsbad, CA). The beads are then resuspended with fluorescein isothiocyanate antibodies from Human Serum (ref F9636; Sigma-Aldrich) at 20 mg/mL and incubated overnight at room temperature. After centrifugation, supernatant is removed, and the beads are washed four times in PBS. PBS is then removed by a final centrifugation step, and the beads are resuspended in 40 μL/coverslip DMEM 4.5 g/L L-glucose without phenol red (ref 31053-028; Life Technologies) at 37°C.

Cell culture

RAW 264.7 murine macrophages (ref 91062702) were purchased from the European Collection of Authenticated Cell Cultures (Public Health England, United Kingdom). They were cultured in T-80 culture flasks (ref 734-2131; VWR International, Radnor, PA) with DMEM 4.5 g/L L-glucose supplemented with 10% fetal calf serum, 1% penicillin-streptomycin, and 2 mM L-Glutamine (ref 10313-021, 10500-056, 31053-028, and 25030024; Life Technologies) at 37°C and 5% CO_2. 24 h before the experiment, they were detached using TryPLE (ref 12605-010; Life Technologies) incubated at 37°C for 5 min and seeded on 22 × 22 mm no. 1.5 glass coverslips (ref 631-0125; VWR International) in six-well plates (ref 734-0054; Corning, Corning, NY) at 1 million cells per well.

Phagocytosis assay with functionalized droplets or beads

Seeded glass coverslips are mounted on an open chamber formed by two coverslips separated by a 0.1-mm-thick double-sided tape, and 2 million droplets or beads suspended in 40 μL DMEM are injected in the chamber. The cells are put upside down on the top of the chamber when incubated with oil droplets so that the less dense droplets go upwards to encounter the cells. The droplets and cells are incubated together for 45 min at 37°C in a cell culture incubator (5% CO_2), then the chamber is rinsed with 160 μL PBS and cells are fixed in 4% paraformaldehyde solution.

Immunostaining

Fixed cells are stained using Hoechst 33258 4 μg/mL (ref H H1399; Life Technologies) and phalloidin Atto 550 20 μM (ref 19083; Sigma-Aldrich) in PBS for 30 min.

Microscopy

Samples were imaged with a confocal Leica TCS SP8 (Wetzlar, Germany), using two hybrid detectors, and a 40×/1.30 NA oil immersion objective. They were illuminated sequentially with four lasers at 405, 488, and 552 nm. Hoechst 33258 and Atto550 were observed simultaneously on different detectors, and Alexa 488 was observed on a separate channel. A prism separated the light, and the LAS X software optimized the window of wavelength gathered for each fluorophore: 410–510 nm for Hoechst 33258, 493–568 nm for Alexa 488, and 557–789 nm for Atto 550.

Automated image analysis

Image analysis was performed with CellProfiler 2 (33) (https://www.cellprofiler.org) using a custom-built pipeline. All obtained data were stored in an SQL database (SQLite3). Further data visualization was performed with Python 3 code using SQLite3 to pass on queries to the database and Matplotlib for plotting. All codes are available upon request.

To evaluate quantitatively the efficiency of the classification, we define $X_{INT} = (TP/TP + FN)$ and $X_{EXT} = (TN/TN + FP)$, where TP and TN stand for the number of true positives (internal droplets) and true negatives (external droplets), respectively, and FP and FN for the number of false-positives (external droplets classified as internal) and false-negatives (internal droplets classified as external). X_{INT} and X_{EXT} correspond to the sensitivity and the specificity, respectively.

Please cite this article in press as: Montel et al., A Multiparametric and High-Throughput Assay to Quantify the Influence of Target Size on Phagocytosis, Biophysical Journal (2019), https://doi.org/10.1016/j.bpj.2019.06.021

RESULTS

We have developed a semiautomatic method for the quantitation of phagocytosis by adherent or semiadherent phagocytes ingesting various phagocytic probes such as polystyrene beads (34) or lipid droplets (35). RAW 264.7 murine macrophages (36) were used as the model cell line, and we focused our study on the FcγR-mediated phagocytosis of IgG-coated fluid and solid microparticles, lipid droplets (35), and polystyrene particles (34), respectively.

Bare or IgG-functionalized particulate targets are presented to phagocytic cells for 45 min in a cell culture incubator. After rinsing the supernatant, cells are fixed, stained, and imaged by confocal scanning microscopy. Both the nucleus and the cytoplasm are stained to perform segmentation of the cells. Here, we use Hoechst 33258 (37) and Atto 555-phalloidin (38) as nuclear and cytoskeletal staining agents, respectively. For each sample, corresponding to a glass coverslip, we observe 10 fields of views, each counting at least 300 cells. Consequently, at least 3000 cells per sample are analyzed and quantified for each condition.

The imaging procedure consists in acquiring each color channel at two specific heights inside the sample using a confocal microscope, as schematized in Fig. 2 *A*: 1) at the basal level where the cell is in contact with the glass, referred to as Z_{low}; and 2) at the midheight level, Z_{high}, inside the cell at a vertical coordinate equal to the radius of the targets. Targets, either beads or lipid droplets, appear in the bright-field channel as disks with a gray center surrounded by the succession of a white ring and a dark ring at the edge, as is visible in Fig. 2 *B*. These rings result from the difference of refractive index with water (39), which is relatively high in the case of soybean oil ($n = 1.47$ (40)) and polystyrene ($n = 1.615$ (41)). The cell and its boundaries are easily discernable on the actin cortex imaging at the basal level, Z_{low}, where the spreading is usually maximal and the intensity more uniform, as shown in Fig. 2 *C*. By contrast, the area occupied by an internalized target appears dark on the cytoplasmic image recorded at the $z = Z_{high}$ midheight level, as shown in Fig. 2 *D*. Dark regions will thus be used afterwards to determine the status of targets regarding their internalization by cells or not.

Cell segmentation

We use a classical approach to proceed with the cell segmentation based on localization of the nuclei and on propagation over the basal actin cortex. Nuclei are first segmented from nuclear stained images at the midheight level, Z_{high} (Fig. 3 *A*), by dividing the image in tiles of one-tenth the image size and applying an intensity threshold obtained by the Otsu method (42) on each tile. Cells are then propagated (43) from the nuclei to their respective cytosol boundaries over on the actin cortex images recorded at the basal level, Z_{low}, as illustrated on Fig. 3 *B*. For individual cells, propagations stop when an abrupt increase or decrease in intensity is detected, which in our case was a sharp decrease at the border of the cytoplasm. When the propagation of one cell encounters the propagation of a neighbor, the border is determined by a balance between the distance to the nucleus and the intensity gradient at the border. Finally, to get rid of dead cells, cellular debris, or potential artifacts, we discard detected objects whose area is under a preselected threshold.

The algorithm creates two numerical objects related to the cell cytoplasm, which will be further used for target classification. The first one, called "Cytoplasm," is created by subtracting the nuclear area from the expanded cell area. The Cytoplasm object corresponds to the cytosol as a whole (i.e., including the internalized target). The second one, called "CytoplasmMinusTargets," corresponds to the actual cytoplasm of the cells, after having removed the overlapping particles from its envelope. We finally label all Cytoplasm and CytoplasmMinusTargets objects and record their positions, some geometric features, and their relationship to internalized droplets in a database.

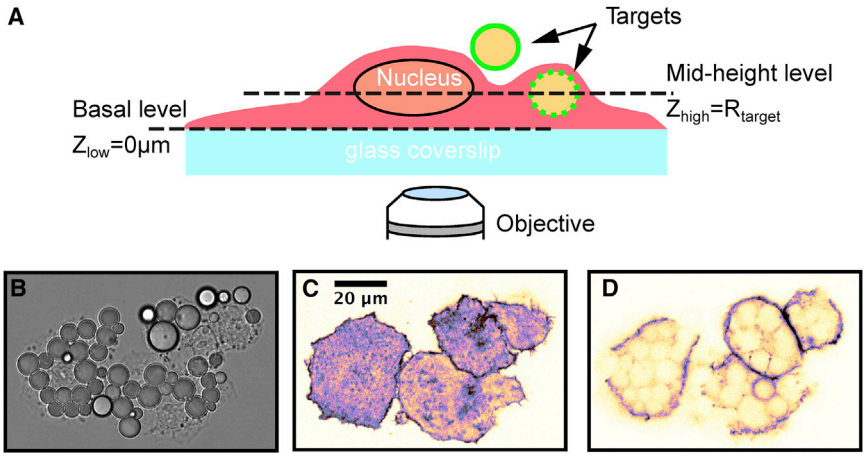

FIGURE 2 (*A*) Schematic representation of the two focal planes imaged by confocal microscopy for analysis. (*B*) A bright-field image of macrophages and droplets at Z_{high} is shown. (*C* and *D*) A confocal image of phalloidin staining of cells at the basal (*C*) and midheight (*D*) levels is shown. The intense basal actin network allows detection of the cell borders, whereas the holes in the cytoskeletal staining at the places where targets are inside the cytoplasm allow one to discriminate internalized targets. Scale bars, 20 μm. To see this figure in color, go online.

Please cite this article in press as: Montel et al., A Multiparametric and High-Throughput Assay to Quantify the Influence of Target Size on Phagocytosis, Biophysical Journal (2019), https://doi.org/10.1016/j.bpj.2019.06.021

Segmentation of the targets

Targets, either lipid droplets or beads, are segmented from bright-field images similar to the one shown in Figs. 3, *A* and *B* and S2. Two features are detrimental to the correct segmentation and eventual classification of the targets: first, for high phagocytic indexes, particles form clusters from which it is difficult to individualize objects; second, we observe out-of-plane targets at the apex of the cell that may be considered as internalized by classification routine detailed in the next paragraph.

Computing the numerical difference of the bright-field images recorded at the basal and midheight levels solves both issues for oil droplets, as shown in Fig. 3 *C*. Indeed, we take advantage of the sharp variation of the diffraction rings around the focal plane of the droplets to discriminate droplets in the midheight plane from droplets above it. Fig. 3 *C* shows that the borders of the in-plane targets on the two images are very different, whereas the borders of the out-of-plane targets are very similar. By computing the difference between the bright-field images, we obtain an image in which the borders of in-plane targets are white, whereas out-of-focus targets appear dark, making the segmentation easy and straightforward. Additionally, the white borders of neighboring droplets are well separated, facilitating the segmentation in crowded regions. To remove small artifacts, we discard acquired targets whose area or form factor is below a preselected threshold. The value of both thresholds depends on the size distribution of targets. Conversely, polystyrene microbeads are simply segmented using a predefined threshold on the bright-field image at the midheight level, Z_{high}, thanks to their bright central area. As for cells, we record the position and size of the targets and store it for further analysis.

Classification of the targets regarding internalization

For a target to be classified as internalized by a phagocytic cell, we consider and evaluate three independent criteria: 1)

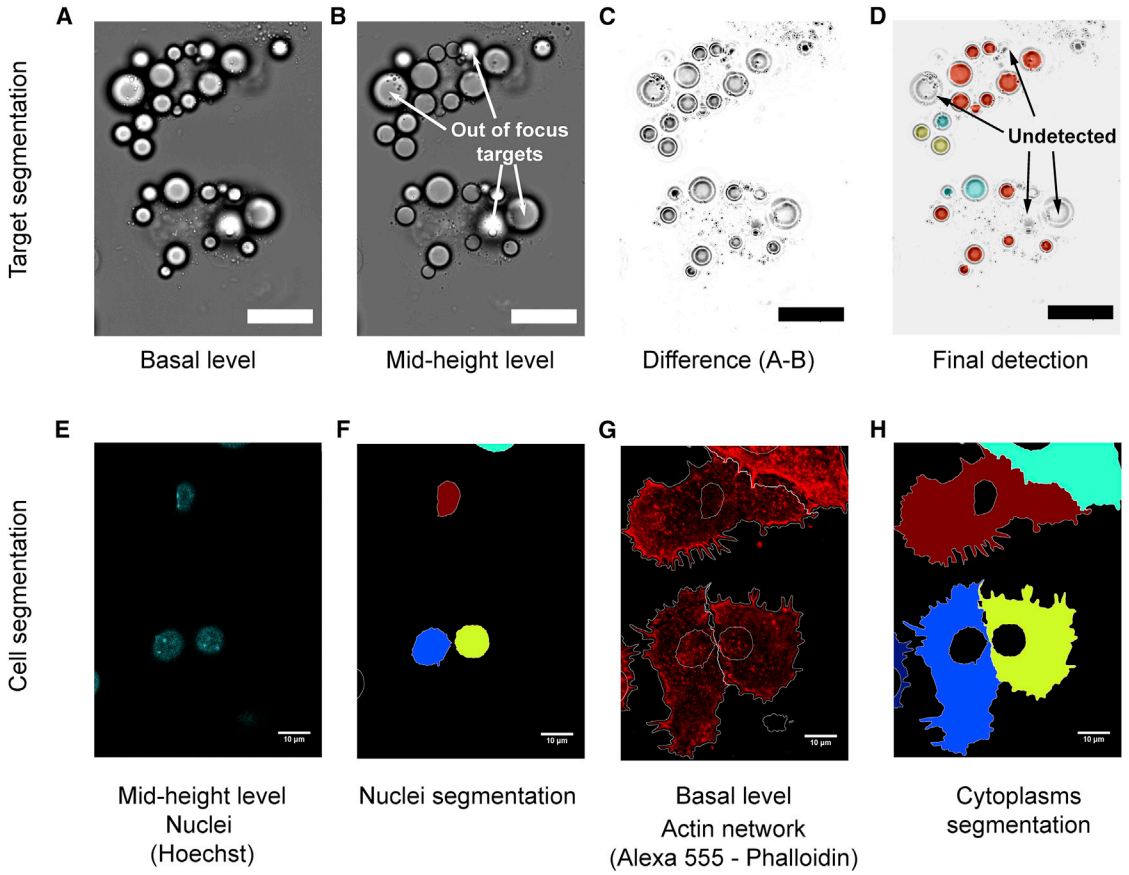

FIGURE 3 Example of the target segmentation routine (*A–D*). The pixelwise difference between the images at two heights (*A* and *B*) is calculated (*C*). On-focus targets have different borders on the two images, whereas out-of-focus targets (*arrows*) are similar. Thus, only on-focus targets appear in white on the difference image. The final classification is shown in (*D*), with red being internalized droplets and all other colors being external droplets. The steps of cell segmentation (*E–H*) are shown: (*E*) nuclei are detected from Hoechst staining at the midheight Z_{high}, (*F*) each nucleus not touching the border is labeled, (*G*) a propagation algorithm detects the cell's border on a phalloidin staining of the actin cytoskeleton at the basal level Z_{low}, (*H*) each cell above the cutoff area is labeled, and cytoplasm objects are created by subtracting the nucleus. To see this figure in color, go online.

Please cite this article in press as: Montel et al., A Multiparametric and High-Throughput Assay to Quantify the Influence of Target Size on Phagocytosis, Biophysical Journal (2019), https://doi.org/10.1016/j.bpj.2019.06.021

the target has to be in the same focal plane as the cell, 2) the target should be localized within the boundaries of the cytoplasm of a segmented cell, and 3) most of the area of the target has to occupy a space inside the cytoplasm, meaning that a dark sport is visible in the actin cortex image recorded at the midheight level. A schematic representation of the classification algorithm is shown in Fig. 4.

The first criterion is assessed during the target segmentation in which out-of-focus targets are discarded by the segmentation routine. As a consequence, all the detected targets meet this criterion because those that do not are discarded before classification. We assess the second criterion by performing a pixelwise multiplication of the binary image of the cell's area and the binary image of the target's area. On the resulting image, the target is considered as internalized following this criterion if more than 80% of its corresponding pixels are located within the border of a single cell. Finally, the third criterion is evaluated on the cytoplasmic image recorded at the midheight level. The mean intensity of the cytoplasmic staining inside the border of each target is measured after normalization of the fluorescence intensity of the image. Areas characterized by an intensity level higher than 10% of the maximal intensity are classified as noninternalized and discarded.

At the end of the process, internalized targets that fulfill the three above criteria are related to the closest Cytoplasm object, that is, the object that contains them. Their features are measured and are stored in the database alongside the unique identifier of the cell they are in.

Database structure and population

During the segmentation and classification, morphological features of the cells and targets are acquired and subsequently stored in a comprehensive SQL database generated by CellProfiler according to our criteria. A diagram of the database is shown in Fig. S3 and details about the fields and categories are summarized in the Supporting Materials and Methods. The shape of nuclei, cells, and targets is measured from the segmented images. Intensity measurements on all fluorescent channels are performed at the basal and midheight level for cell cytoplasms. In addition, intensity measurements are performed on targets at the midheight level.

At the end of this protocol, we obtain a pipeline for phagocytic assays that takes confocal images of the phagocytes and targets as input and provides a database containing measurements on cells and targets, as well as the relationships between a cell and its internalized targets.

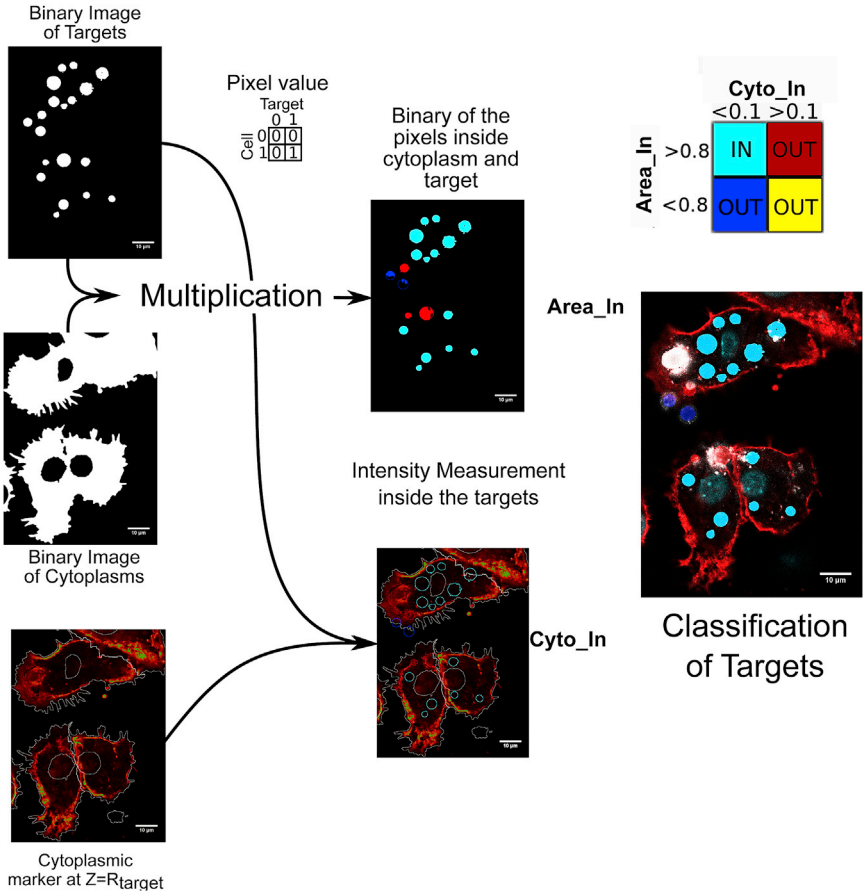

FIGURE 4 Schematic representation of the classification algorithm that detects internalized targets. Binary images of the segmented targets and cytoplasms are multiplied bitwise so that only the pixels both inside a target and a cytoplasm are one. The mean value of the pixels of the multiplied image is measured over the whole target, giving a measurement of the percentage of the target area that is inside a cytoplasm. Meanwhile, the value of cytoplasmic staining inside the target is measured. If more than 80% of the target area is in the cytoplasm and the cytoplasmic staining is under a threshold, then the target is deemed internalized (in *cyan*). Targets displaying too high actin staining (in *red*) are usually above the cell or being internalized, whereas targets not overlapping the cytoplasm are either outside (in *blue*) or bordering (in *yellow*) the cell. To see this figure in color, go online.

Please cite this article in press as: Montel et al., A Multiparametric and High-Throughput Assay to Quantify the Influence of Target Size on Phagocytosis, Biophysical Journal (2019), https://doi.org/10.1016/j.bpj.2019.06.021

Efficiency of the segmentation routine

To assess the efficiency of the detection and classification algorithm, its results were confronted to a blind manual counting and classification on three randomly chosen images from each of three replicate coverslips. Table 1 summarizes the results of the algorithm for three sizes of beads (3, 6, and 10 μm diameter) and three sizes of droplets (3, 5.5, and 8 μm diameter). X_{INT} (i.e., the part of the targets that are correctly classified as internalized) ranges from 87 to 99%, with a score increasing with size. X_{EXT} (i.e., the part of external targets correctly classified) ranges from 77 to 94%, increasing with size. The definition of X_{INT} and X_{EXT} are given in the Materials and Methods.

Influence of target size on phagocytic efficiency

The database structure allows us to extract complex information from our experiments for a large number of cells ($n > 3000$). More specifically, we used the algorithm to study the influence of the target size on the phagocytosis efficiency. We first measured the phagocytic efficiency of monodisperse populations of droplets (diameters: 3, 5.5, and 8 μm), both for the case of uncoated targets and targets coated with fluorescent IgGs. The droplets are saturated with IgGs to prevent the formation of contact clusters of IgG at the surface of the droplets. Because the size of the clusters would depend on the size of the droplet, cluster formation would interfere with the assessment of a size effect on phagocytosis. For all experimental conditions, we worked with more targets than the theoretical uptake for a given size.

Fig. 5 *A* shows that phagocytosis of IgG-coated droplets is five times more efficient than for the case of noncoated droplets. The graph shows that both nonspecific and specific internalization is higher for smaller droplets, which is confirmed in Fig. 5 *B* by the linear increase of the phagocytic index with the inverse of target surface, both for coated and uncoated targets. Moreover, Fig. S6 shows that latrunculin B and wortmannin (44) impair the uptake of 8 μm large IgG-coated droplets.

Fig. 5 *C* represents the distribution of the total wrapped surface by cells containing at least one droplet for the three sizes of monodisperse droplets and the polydisperse emulsion. Under 200 μm^2 of total wrapped surface (i.e., the surface of one 8 μm diameter droplet), the distributions are dependent on the size of droplets. Indeed, cells cannot internalize a surface smaller than the minimal size of the targets available in the culture medium. On the contrary, the four distributions are strikingly similar for a total internalized surface greater than 200 μm^2, as can be seen on Fig. S7, meaning that the total surface area cells can internalize is independent on the size of the targets.

Finally, to test the existence of a preferred size in a competitive context and check for synergetic effects related to the presence of targets differing by size, we performed the experiments and quantified it for the case of naked and IgG-coated polydisperse droplets ranging from 2 to 15 μm. Fig. 5 *D* shows that the size distribution of internalized droplets is identical to the initial droplet size distribution, meaning that all sizes of droplets are equally represented among internalized targets and that no size is favored by the macrophages.

DISCUSSION

In this work, we present the design of a semiautomatic method based on confocal microscopy, image analysis, and the use of a database for the quantitative analysis of phagocytosis assays. The algorithm yields comprehensive data on cells, targets, and their respective geometric and fluorescence parameters. It automatically discriminates internalized from external particles and finally stores the relationships between cells and particles that experience uptake. Currently, the method is able to analyze samples of up to 3000 cells and is only limited by the microscopic imaging because this part is performed manually. As compared to manual counting, we gain at least one order of magnitude (28,29) in terms of sample size. In addition, unlike methods published so far, the experimental procedure does not require staining the targets for the segmentation. This means that the method makes it possible to analyze the signal associated to nonspecific phagocytosis, that is, the one measured for negative control experiments.

The automatic analysis procedure is divided in three main steps: segmentation of the cells, segmentation of the targets, and classification of the targets as internalized or external. The procedure is thus based on the image recording over three channels (bright field for the targets, fluorescence of Hoechst for the nuclei, and fluorescence of phalloidin for

TABLE 1 Estimation of the Efficiency of the Algorithm for Detection and Classification of Microbeads

Diameter of Target	Bead (3 μm)	Bead (6 μm)	Bead (10 μm)	Droplet (3 μm)	Droplet (5.5 μm)	Droplet (8 μm)
Detection rate	88%	93%	97%	83%	92%	94%
Error rate	0%	4.7%	0.6%	1.2%	0.5%	0.3%
X_{INT} (sensitivity)	99%	95%	92%	88%	87%	87%
X_{EXT} (specificity)	89%	94%	90%	77%	89%	90%

Detection rate is the number of detected targets among the targets identified by the human eye. Error rate is the number of nontarget objects detected by the algorithm. X_{INT} is the number of targets correctly classified as internalized by the machine among the targets internalized as determined by the observer. X_{EXT} is the number of targets correctly classified as external by the machine among the targets external as determined by the observer.

Please cite this article in press as: Montel et al., A Multiparametric and High-Throughput Assay to Quantify the Influence of Target Size on Phagocytosis, Biophysical Journal (2019), https://doi.org/10.1016/j.bpj.2019.06.021

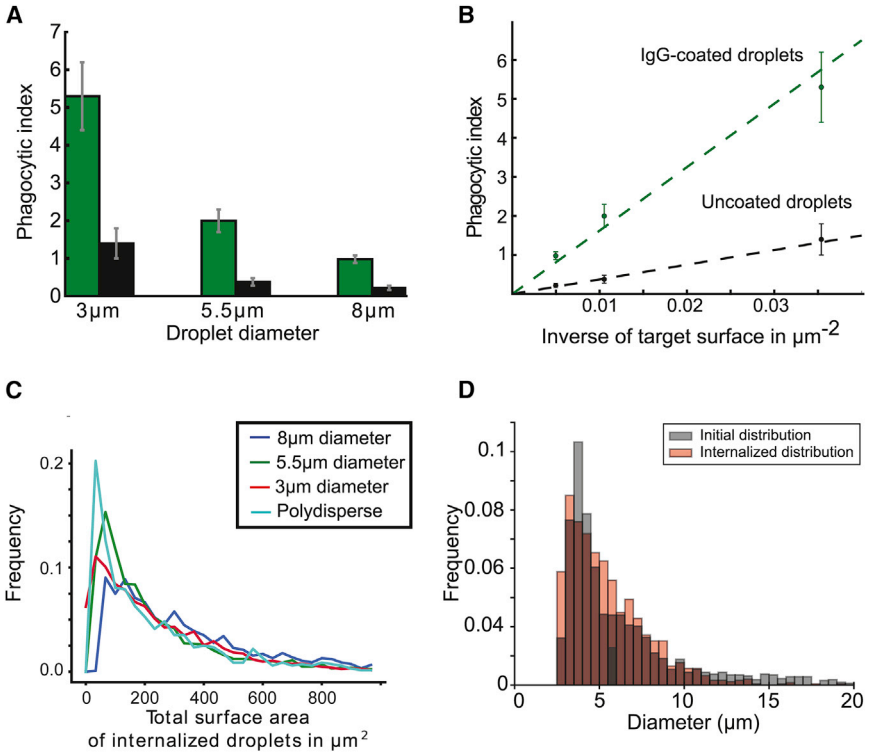

FIGURE 5 (*A*) Phagocytic index for three sizes of monodisperse droplets with (*green*) and without (*black*) IgG coating. (*B*) The phagocytic index as a function of the inverse of droplet surface is shown. Both coated and uncoated droplets are internalized proportionally to the inverse of target surface. (*C*) Shown is a histogram of the total engulfed surface for three monodisperse emulsions and one polydisperse emulsion, obtained by summing the surface area of the droplets in each cell. The shape of the distributions for surfaces superior to 200 μm^2 (surface of one 8 μm droplet) was compared using a two-sample Kolmogorov-Smirnov test and did not significantly differ for any pair of distributions ($p > 0.05$). (*D*) Shown is a histogram of internalized droplets (*red*) as compared to the initial size distribution of the polydisperse droplets, measured before performing the assay (*gray*). The two histograms show no significant differences (Kolmogorov-Smirnov two-sample test; $p > 0.05$). To see this figure in color, go online.

the cytoplasms). The detected nuclei served as seeds that propagate into the cytoplasm and stop at the borders of the cells. Over the remaining channels, proteins of interest can be labeled, and the intensity and localization of their fluorescence are assessed on the images at the two levels. As an example, we imaged the fluorescent antibodies Alexa 488 antibiotin IgGs that coat the droplets and stained the cells for Fcγ receptors using anti-Cd16/Cd32 antibodies, as can be seen in Fig. S4. As a variant, when the coating on the targets is not saturated, the remaining biotins on the surface of external droplets (20) can be coated with fluorescent streptavidin, providing an additional signal to discriminate adherent droplets from internal droplets, as illustrated in Fig. S5.

A correct segmentation of the cells is a necessary condition to get a good classification because the main determinant of the classification is the overlap between cytoplasmic and target areas. Our approach here is similar to (24,25) and allows measuring the morphology of the cells. The stained nuclei are segmented first using thresholding; the cytoplasms are then propagated from the nuclei according to the method developed by Jones et al. (43). The use of a confocal microscope conjugated to phagocytic cells added several subtleties to this classical approach because the presence of internalized targets causes dark areas inside the cytoplasm. Firstly, the detection of cell borders from the cytoplasmic stain has to be performed on the basal level of cells where the signal from the actin cytoskeleton is higher and more uniform. Secondly, the darker areas in the higher plane can then be exploited to confirm the internalization of targets.

Regarding target detection and classification, two main strategies emerge from the literature. The first one is to classify internal and external targets by staining them differently. The cells and targets are fixed at the end of the phagocytic assay, and a staining step labels external targets only. All targets are detected, either using a prefixation stain (20–22) or bright-field images (23). The classification is thus performed before the imaging step, and the detection is performed subsequently on both populations of targets. This protocol, although limiting greatly the risk of errors in classification, is only usable on fixed samples and solid objects. On lipid droplets, the initial staining of the droplets can cluster in contact with cells and is extracted from the surface after internalization making it impossible to detect reliably droplets from a prior staining. Moreover, the post hoc external staining is only possible on nonsaturated droplets because it relies on the staining of remaining available biotins by streptavidin, as illustrated in Fig. S5, and it is not as efficient because of the liquid nature of the interface. Finally, if one needs to relate one cell to its internalized targets, it is still necessary to segment the cell contours and to examine the overlap between the cytoplasms and the targets. We chose instead to use the overlap between the segmented cells and targets as the main criterion for classification, as in (24,25). The difference in our approach was to use the bright-field images at the two planes Z_{high} and Z_{low} to segment the targets. It has two advantages: first, to be

Please cite this article in press as: Montel et al., A Multiparametric and High-Throughput Assay to Quantify the Influence of Target Size on Phagocytosis, Biophysical Journal (2019), https://doi.org/10.1016/j.bpj.2019.06.021

efficient even in crowded environments, where threshold-based segmentation would fail to separate targets, and second, to exclude out-of-focus targets, reducing false-positive rates, while simultaneously reducing the number of fluorescence channels necessary for the automation. This strategy for cell and target segmentation requires only two stains for cell labeling and none for the targets, whereas most of the alternative protocols required at least three: either two for the cells and one for the targets (24,25) or one for the cells and two for the targets (20–22). Moreover, the phagocytosis of targets without staining of any kind can be assessed using this strategy because it requires no labeling and provides large number of cells to analyze to compensate for the low uptake of nonopsonized particles. In our case, experiments were performed of fixed samples, but as long as the dyes are compatible with cells, the same protocol could be used on images taken from live cells.

The classification of targets as internalized or not is performed on segmented cells and targets using two criteria: the overlap between cytoplasms and targets and the low cytoplasmic staining at the location of the target. The second criterion requires confocal imaging and is useful to exclude adherent targets or targets being internalized as the samples were fixed, in which case, the cytoskeleton is well developed around the target or targets above the cell where the overlap is positive but the cytoplasmic staining is visible inside the target projected area. X_{INT} (i.e., the part of targets correctly classified as internalized) ranges from 92 to 99% for beads and around 87% for droplets, with a score decreasing with size. X_{EXT} (i.e., the part of targets correctly classified as external) ranges from 89 to 94% for beads and from 77 to 90% for droplets. Because IgGs cluster at the contact site with cells, droplets adhere more to macrophages than beads do. Adherent droplets often surround macrophages, increasing the number of false-positives and false-negatives during the classification step as compared to beads. The two measurements depend on one another: when criteria for internalized targets are made more precise, more and more targets are incorrectly classified as external, and the gain in sensitivity is compensated by a loss in specificity. Because we favored sensitivity over specificity, we tend to overestimate the phagocytic indexes. However, the error on the phagocytic index due to misclassification is lower than the variability from one biological sample to another, which diminishes the gain that would be obtained by optimizing further the classification algorithm.

The final database stores measurements for cells, targets, and the relationship between the two. It enables any cell to have access to the measurements made on the targets it contains or, conversely, any target to have access to the measurements on the cell it is in or on the other targets internalized with it. The ability to connect the cells and targets makes it possible to draw a lot of information from assays using polydisperse targets. Here, it was used to compute for each cell the total area of engulfed targets and confirm that in a population of cells, the distribution of internalized total area does not depend on the area of the targets. It can be used to sort cells based on the properties of the targets they have internalized and thus broaden the scope of hypotheses that can be tested.

Experiments with monodisperse and polydisperse emulsions lead to apparently contradictory results: smaller monodisperse targets are more often internalized, whereas the size distribution is unchanged for polydisperse targets, with the cells showing no preference for smaller targets. The phagocytic index dependence in size is the same for coated and uncoated targets, and it is linearly proportional to the inverse of the targets' area for both, differing only by the slope. Thus, the product of the number of internalized objects and of the area of said objects (i.e., the mean total surface area internalized by cells) is a constant. This constant however depends on the coating of the targets because nonspecific and specific curves have a different slope (Fig. 5 *B*).

In 1988, Simon and Schmid-Schönbein (28) proposed a simple geometrical model, postulating that membrane surface availability was the limiting factor of phagocytosis. During phagocytosis, the engulfed particle is wrapped closely in the phagosome, and the available cell membrane is consequently reduced, whereas the cell volume increases. Simon and Schmid-Schönbein (28) measured the initial surface and volume of neutrophils and assumed that at maximal uptake, the cells would round up to minimize their surface. They derive a theoretical phagocytic index depending on measured initial cell volume and surface, on target size, and on the addition of surface from compartment reservoirs. This model agrees with our observations that the total surface area of internalized objects is constant.

Starting from the existing literature, we compiled or computed the quantitative phagocytic indexes measured for opsonized targets of different nature and various cell types. These experimental results are plotted along our own measurements in Fig. 6 as a function of the inverse of target surface area. In addition, we added a curve corresponding to a theoretical model from Simon and Schmid-Schönbein (28). Whereas results for targets within 3–10 μm ranges are consistent with our own and with each other, results for smaller targets are not. However, the highest measured phagocytic index aligned well with those of larger targets and with the theoretical prediction. At smaller sizes, the theoretical uptake is above 100 targets per cell, yet cells were not always provided with that many particles. In Fig. 6, we circled in red every experiment in which the cells were not provided with at least five times the theoretical maximum of targets, a situation that could result from a shortage of targets, leading to cells not being able to reach their maximal uptake. Circled results are also the ones that differed from theoretical prediction. It is to be noted that Fig. 6 brings together results obtained

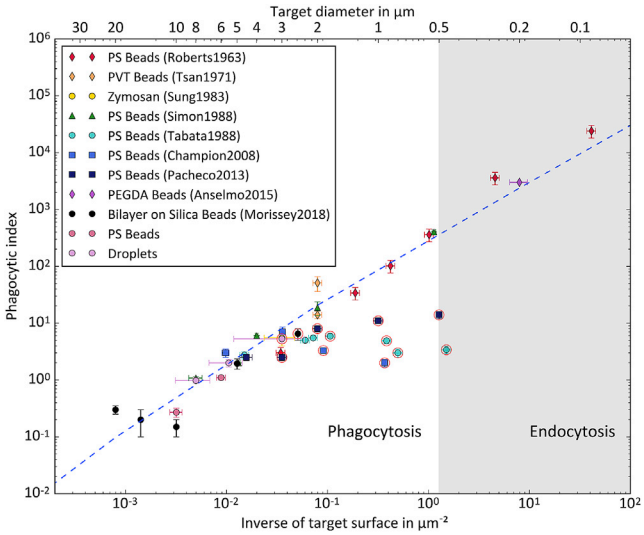

FIGURE 6 Phagocytic index as a function of the inverse of opsonized target surface as collected from the literature (15–19,26–29) and our experiments. A theoretical prediction from Simon and Schmid-Schönbein (28) is shown with the dotted blue line. Experiments in which the ratio of supplied opsonized particles to their theoretical uptake value is smaller than 5 are circled in red. This corresponds to experiments whose final result is not limited by the cell surface area but rather by an insufficient number of particles presented to the cells. To see this figure in color, go online.

with several different experimental methods for six types of cells, adherent or in suspension, and four types of targets (see Table S1 for details).

Previous experiments addressing the influence of size on phagocytosis were always performed with monodisperse objects, presumably because of the constraints of data collection. To our knowledge, they were never focused on the quantitative comparison of a possible competition among the presence of several particles of different sizes during the same experiment in the phagocytic context. The main improvement of the technique we designed is to give access to the individual objects' measurements for both cells and targets, as well as their relationship. We thus performed experiments using polydisperse emulsions and subsequently measured the size distribution of internalized objects. Should the cells prefer internalizing targets of a specific range of size, the distribution of internal targets would be skewed to reflect the preference. When presented with a polydisperse emulsion, cells display no preference for one size over another because the size distribution of targets is conserved by internalization. This results in an apparent contradiction: no preferred size is observed in a competitive context, whereas the smaller monodisperse targets are more often internalized. We can also compute, at an individual level, the total area of the targets internalized by each cell. For the three sizes of droplets, the distribution of mobilized surface per cell is similar, with more small targets internalized per cell as to compensate for their smaller surface.

Taken together, these results point toward a surface limitation rather than a preference for a target diameter: cells internalize targets they encounter up to their available surface, regardless of the target size as long as the surface can be mobilized. This surface is measured around 200 μm^2, the same order of magnitude as the estimated cell's own surface (28), and can be mobilized in a matter of minutes, as can be seen in Video S1. Smaller objects are not internalized in larger numbers because their size is more favorable but because it requires more of them before reaching the limit of surface the cell can mobilize. This is also consistent with experimental results from (11,45,46), which showed available membrane is a limiting factor for phagocytosis and that reaching the surface limit triggers degranulation. The scaling in surface is remarkably maintained between phagocytes of different cell types and for objects of different nature and coating as long as they are opsonized. It is interesting to note that this relationship is also maintained for uncoated objects internalized by macrophages through other receptors, with a lower total surface limitation: it could point toward membrane availability being dependent on receptor activation (e.g., through the exocytosis of surface) (11,28,47,48). One of the parameters regulating the selectivity of phagocytosis could then be the controlled delivery of membrane surface by activated receptors.

Finally, our results point to the fact that the surface of objects is an essential parameter to take into account when one designs a phagocytic assay. Because surface is a determinant parameter of maximal uptake, the phagocytosis of objects of diverse shapes and sizes should only be compared between objects of equal surface.

CONCLUSIONS

This method combines the advantages of several of the previous protocols: no staining of the targets is required and geometrical and intensity parameters are measured on cells and targets. It also adds a layer of information by storing the relationship between the objects, allowing much more complex observations. The data collected during experiments on the role of size in phagocytosis shed a new, to our knowledge, light on results previously reported in the literature. Using polydisperse emulsion droplets and individual target and cell measurements, we concluded that macrophages engulfed targets regardless of size until they reach a fixed internalized surface. A review of more than 50 years of experiments on the role of size concurs to show this surface limitation as the main predictor of the phagocytic uptake regardless of cell types or the nature of targets.

SUPPORTING MATERIAL

Supporting Material can be found online at https://doi.org/10.1016/j.bpj.2019.06.021.

Please cite this article in press as: Montel et al., A Multiparametric and High-Throughput Assay to Quantify the Influence of Target Size on Phagocytosis, Biophysical Journal (2019), https://doi.org/10.1016/j.bpj.2019.06.021

AUTHOR CONTRIBUTIONS

L.M. and J.F. designed the study, analyzed the data, and wrote the manuscript. L.M. and L.P. did the experiments. L.M. developed the quantitation algorithm.

ACKNOWLEDGMENTS

We thank Nicolas Carpi (Bio6 team, UMR 144, Institut Curie) for his help on the software.

This work has received support of the Institut Pierre-Gilles de Gennes (Laboratoire d'excellence: ANR-10-LABX-31; Investissements d'avenir: ANR-10-IDEX-0001-02 PSL and Equipement d'excellence: ANR-10-EQPX-34). The authors acknowledge funding from the Agence Nationale de la Recherche, under grant ANR 15-CE18-0014-01 (PHAGODROP).

REFERENCES

1. Rosales, C., and E. Uribe-Querol. 2017. Phagocytosis: a fundamental process in immunity. *BioMed Res. Int.* 2017:9042851.
2. Wright, A., and S. Douglas. 1904. Opsonins. *Proc. R. Soc. Lond.* 73:128–142.
3. Ward, H. K., and J. F. Enders. 1933. An analysis of the opsonic and tropic action of normal and immune sera based on experiments with the pneumococcus. *J. Exp. Med.* 57:527–547.
4. Fleisch, H., R. G. Russell, and F. Straumann. 1966. Effect of pyrophosphate on hydroxyapatite and its implications in calcium homeostasis. *Nature.* 212:901–903.
5. Malawista, S. E., J. B. Gee, and K. G. Bensch. 1971. Cytochalasin B reversibly inhibits phagocytosis: functional, metabolic, and ultrastructural effects in human blood leukocytes and rabbit alveolar macrophages. *Yale J. Biol. Med.* 44:286–300.
6. Levin, R., S. Grinstein, and D. Schlam. 2015. Phosphoinositides in phagocytosis and macropinocytosis. *Biochim. Biophys. Acta.* 1851:805–823.
7. Arkin, A. 1913. The influence of strychnine, caffeine, chloral, antipyrin, cholesterol and lactic acid on phagocytosis. *J. Infect. Dis.* 13:408.
8. Fenn, W. O. 1922. Effect of the hydrogen ion concentration on the phagocytosis and adhesiveness of leucocytes. *J. Gen. Physiol.* 5:169–179.
9. Huang, K. Y., R. M. Donahoe, …, H. R. Dressler. 1971. Enhancement of phagocytosis by interferon-containing preparations. *Infect. Immun.* 4:581–588.
10. Beningo, K. A., and Y. L. Wang. 2002. Fc-receptor-mediated phagocytosis is regulated by mechanical properties of the target. *J. Cell Sci.* 115:849–856.
11. Masters, T. A., B. Pontes, …, N. C. Gauthier. 2013. Plasma membrane tension orchestrates membrane trafficking, cytoskeletal remodeling, and biochemical signaling during phagocytosis. *Proc. Natl. Acad. Sci. USA.* 110:11875–11880.
12. Garapaty, A., and J. A. Champion. 2017. Tunable particles alter macrophage uptake based on combinatorial effects of physical properties. *Bioeng. Transl. Med.* 2:92–101.
13. Fenn, W. O. 1922. The temperature coefficient of phagocytosis. *J. Gen. Physiol.* 4:331–345.
14. Leishman, W. B. 1902. Note on a method of quantitatively estimating the phagocytic power of the leucocytes of the blood. *Br. Med. J.* 1:73–75.
15. Roberts, J., and J. H. Quastel. 1963. Particle uptake by polymorphonuclear leucocytes and ehrlich ascites-carcinoma cells. *Biochem. J.* 89:150–156.
16. Tsan, M. F., and R. D. Berlin. 1971. Effect of phagocytosis on membrane transport of nonelectrolytes. *J. Exp. Med.* 134:1016–1035.
17. Anselmo, A. C., M. Zhang, …, S. Mitragotri. 2015. Elasticity of nanoparticles influences their blood circulation, phagocytosis, endocytosis, and targeting. *ACS Nano.* 9:3169–3177.
18. Champion, J. A., A. Walker, and S. Mitragotri. 2008. Role of particle size in phagocytosis of polymeric microspheres. *Pharm. Res.* 25:1815–1821.
19. Pacheco, P., D. White, and T. Sulchek. 2013. Effects of microparticle size and Fc density on macrophage phagocytosis. *PLoS One.* 8:e60989.
20. Steinberg, B. E., C. C. Scott, and S. Grinstein. 2007. High-throughput assays of phagocytosis, phagosome maturation, and bacterial invasion. *Am. J. Physiol. Cell Physiol.* 292:C945–C952.
21. DeLoid, G. M., T. H. Sulahian, …, L. Kobzik. 2009. Heterogeneity in macrophage phagocytosis of *Staphylococcus aureus* strains: high-throughput scanning cytometry-based analysis. *PLoS One.* 4:e6209.
22. Kraibooj, K., H. Schoeler, …, M. T. Figge. 2015. Automated quantification of the phagocytosis of *Aspergillus fumigatus* conidia by a novel image analysis algorithm. *Front. Microbiol.* 6:549.
23. Yeo, J. C., A. A. Wall, …, N. A. Hamilton. 2013. High-throughput quantification of early stages of phagocytosis. *Biotechniques.* 55:115–124.
24. Al-Ali, H., H. Gao, …, R. Brambilla. 2017. High content analysis of phagocytic activity and cell morphology with PuntoMorph. *J. Neurosci. Methods.* 291:43–50.
25. Song, O. R., N. Deboosere, …, P. Brodin. 2017. Phenotypic assays for *Mycobacterium tuberculosis* infection. *Cytometry A.* 91:983–994.
26. Sung, S. S., R. S. Nelson, and S. C. Silverstein. 1983. Yeast mannans inhibit binding and phagocytosis of zymosan by mouse peritoneal macrophages. *J. Cell Biol.* 96:160–166.
27. Tabata, Y., and Y. Ikada. 1988. Effect of the size and surface charge of polymer microspheres on their phagocytosis by macrophage. *Biomaterials.* 9:356–362.
28. Simon, S. I., and G. W. Schmid-Schönbein. 1988. Biophysical aspects of microsphere engulfment by human neutrophils. *Biophys. J.* 53:163–173.
29. Morrissey, M. A., A. P. Williamson, …, R. D. Vale. 2018. Chimeric antigen receptors that trigger phagocytosis. *eLife.* 7:e36688.
30. Mason, T. G., and J. Bibette. 1997. Shear rupturing of droplets in complex fluids. *Langmuir.* 13:4600–4613.
31. Pinon, L., L. Montel, …, J. Fattaccioli. 2018. Kinetically enhanced fabrication of homogeneous biomimetic and functional emulsion droplets. *Langmuir.* 34:15319–15326.
32. Efremova, N. V., B. Bondurant, …, D. E. Leckband. 2000. Measurements of interbilayer forces and protein adsorption on uncharged lipid bilayers displaying poly(ethylene glycol) chains. *Biochemistry.* 39:3441–3451.
33. Carpenter, A. E., T. R. Jones, …, D. M. Sabatini. 2006. CellProfiler: image analysis software for identifying and quantifying cell phenotypes. *Genome Biol.* 7:R100.
34. Chow, C. W., G. P. Downey, and S. Grinstein. 2004. Measurements of phagocytosis and phagosomal maturation. *Curr. Protoc. Cell Biol.* Chapter 15:Unit 15.7.
35. Ben M'Barek, K., D. Molino, …, J. Fattaccioli. 2015. Phagocytosis of immunoglobulin-coated emulsion droplets. *Biomaterials.* 51:270–277.
36. Raschke, W. C., S. Baird, …, I. Nakoinz. 1978. Functional macrophage cell lines transformed by Abelson leukemia virus. *Cell.* 15:261–267.
37. Latt, S. A., and G. Stetten. 1976. Spectral studies on 33258 Hoechst and related bisbenzimidazole dyes useful for fluorescent detection of deoxyribonucleic acid synthesis. *J. Histochem. Cytochem.* 24:24–33.
38. Wulf, E., A. Deboben, …, T. Wieland. 1979. Fluorescent phallotoxin, a tool for the visualization of cellular actin. *Proc. Natl. Acad. Sci. USA.* 76:4498–4502.

Please cite this article in press as: Montel et al., A Multiparametric and High-Throughput Assay to Quantify the Influence of Target Size on Phagocytosis, Biophysical Journal (2019), https://doi.org/10.1016/j.bpj.2019.06.021

39. Cheong, F. C., B. Sun, …, D. G. Grier. 2009. Flow visualization and flow cytometry with holographic video microscopy. *Opt. Express.* 17:13071–13079.

40. Majors, K. R., and R. T. Milner. 1939. Relation between the iodine number and refractive index of crude soybean oil. *Oil & Soap.* 16:228–231.

41. Boundy, R. H. 1952. Styrene: Its Polymers, Copolymers, and Derivatives. Reinhold, New York.

42. Otsu, N. 1979. A threshold selection method from gray-level histograms. *IEEE Trans. Syst. Man Cybern.* 20:62–66.

43. Jones, T. R., A. Carpenter, and P. Golland. 2005. Voronoi-based segmentation of cells on image manifolds. *In* Computer Vision for Biomedical Image Applications. Y. Liu, T. Jiang, and C. Zhang, eds. Springer, pp. 535–543.

44. Cox, D., C. C. Tseng, …, S. Greenberg. 1999. A requirement for phosphatidylinositol 3-kinase in pseudopod extension. *J. Biol. Chem.* 274:1240–1247.

45. Hackam, D. J., O. D. Rotstein, …, S. Grinstein. 1998. v-SNARE-dependent secretion is required for phagocytosis. *Proc. Natl. Acad. Sci. USA.* 95:11691–11696.

46. Holevinsky, K. O., and D. J. Nelson. 1998. Membrane capacitance changes associated with particle uptake during phagocytosis in macrophages. *Biophys. J.* 75:2577–2586.

47. Samie, M., X. Wang, …, H. Xu. 2013. A TRP channel in the lysosome regulates large particle phagocytosis via focal exocytosis. *Dev. Cell.* 26:511–524.

48. Masters, T. A., M. P. Sheetz, and N. C. Gauthier. 2016. F-actin waves, actin cortex disassembly and focal exocytosis driven by actin-phosphoinositide positive feedback. *Cytoskeleton (Hoboken).* 73:180–196.